Available online at www.sciencedirect.com
SCIENCE DIRECT®
ELSEVIER
International Journal of Mechanical Sciences 46 (2004) 585–608
International Journal of MECHANICAL SCIENCES
www.elsevier.com/locate/ijmecsci

Collapse mechanisms of sandwich beams with composite faces and a foam core, loaded in three-point bending. Part II: experimental investigation and numerical modelling

Craig A. Steeves, Norman A. Fleck*

Cambridge University Engineering Department, Trumpington Street, Cambridge, CB2 1PZ, UK

Received 26 November 2003; received in revised form 30 April 2004

Abstract

This study focuses on the competing collapse mechanisms for simply supported sandwich beams with composite faces and a PVC foam core subjected to three point bending. The faces comprise Hexcel Fibredux 7781-914G woven glass fibre-epoxy prepreg, while the core comprises closed cell Divinycell PVC foam of relative density 6.6% and 13.3%. The mechanical properties of the face sheets and core are measured independently. Depending upon the geometry of the beam and the relative properties of the constituents, collapse is by core shear, face sheet microbuckling or by indentation beneath the middle loading roller. A systematic series of experiments and finite element simulations have been performed in order to assess the accuracy of simple analytic expressions for the strength. In general, the analytic expressions for peak load are adequate; however, simple beam theory becomes inappropriate and the analytic models are inaccurate for stubby beams with thick faces relative to the core thickness. A failure mechanism map is constructed to reveal the dependence of the dominant collapse mechanism upon the geometry of the beam.

Keywords: Sandwich materials; Indentation; Analytical solutions; Optimisation; Bending; Buckling failure; Composite materials

1. Introduction

Sandwich beams are used increasingly in applications requiring high bending stiffness and strength combined with low weight. The sandwich beam concept is that stiff faces, carrying axial and bending loads of the beam, are separated by a lightweight core which carries the shear loads. This idea dates back to the 1820s [1], but the systematic use of sandwich beams and sandwich panels as structural

* Corresponding author. Tel.: +44-1223-332-650; fax: +44-1223-332-662.
E-mail address: naf1@eng.cam.ac.uk (N.A. Fleck).

0020-7403/$ - see front matter © 2004 Elsevier Ltd. All rights reserved.
doi:10.1016/j.ijmecsci.2004.04.004

elements only gained acceptance in the middle of the 20th century for lightweight components of aircraft structures. A recent review of the mechanics of sandwich panels is provided by Zenkert [1], building on the pioneering work of Allen [2] and Plantema [3]. It has long been recognised that sandwich beams fail by a number of competing mechanisms; Gibson and Ashby [4] generated collapse mechanism maps for beams in bending to show the dependence of failure mode upon the geometry of beam and the strength of the faces and core. Their approach was demonstrated for aluminium alloy face sheets and polymeric foam cores, and has since been extended by a number of research groups [5–7] to include the failure modes exhibited by solid metal face sheets and metallic foam cores. The purpose of the present paper is to explore the competing collapse modes for sandwich beams which have been manufactured from woven glass fibre-epoxy face sheets and a PVC foam core, and loaded in three-point bending. This material combination finds widespread application in boat and ship building. The measured collapse response is used to validate the predictions of both analytical models presented in Steeves and Fleck [8], and of finite element simulations given here.

The scope of the paper is as follows. First, analytical predictions for the stiffness and strength of sandwich beams in three-point bending are reviewed briefly from the companion study of Steeves and Fleck [8], and failure mechanism maps are generated from these formulae. A finite element procedure is then used to obtain numerical predictions for the load versus displacement response of selected sandwich beams. The chosen material system is Hexcel Fibredux woven glass-epoxy composite face sheets and three densities of Divinycell PVC foam core. Experiments are performed in order to explore the dependence of failure mode upon geometry and density of core, and to determine the accuracy of the numerical and analytical predictions. Particular attention is given to validating the indentation model presented in Steeves and Fleck [8].

2. Analytic formulae for the stiffness and strength of sandwich beams in three-point bending

Consider a simply supported sandwich beam loaded in three-point bending by circular cylindrical rollers as sketched in Fig. 1. The mid-point of the beam deflects by a transverse displacement u due to the applied load P of the mid-roller. Let L be the beam length between the supports, H the overhang at each end, b the width of the beam, c the core thickness, and t_f be the face thickness. The relevant mechanical properties of the isotropic core are the Young's modulus E_c, shear modulus G_c, compressive strength σ_c, and shear strength τ_c; for the face sheets, the pertinent properties are the axial compressive strength σ_f and axial Young's modulus E_f. Collapse of the beam occurs by

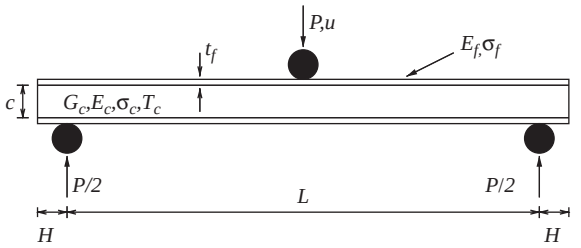

Fig. 1. Geometry of a sandwich beam in three-point bending.

one of several competing mechanisms; the operative failure mode is dictated by the geometry of the beam and the mechanical properties of the face and core materials.

2.1. Stiffness

Allen [2] gives the total deflection u at the mid-point of a simply supported sandwich beam loaded in three-point bending as the sum of the deflections due to bending of the face sheets and shear of the core:

$$u = \frac{PL^3}{48(EI)_{eq}} + \frac{PL}{4(AG)_{eq}}, \tag{1}$$

where $(EI)_{eq}$ is the equivalent flexural rigidity:

$$(EI)_{eq} = \frac{E_f b t_f d^2}{2} + \frac{E_f b t_f^3}{6} + \frac{E_c b c^3}{12} \approx \frac{E_f b t_f d^2}{2} \tag{2}$$

and $(AG)_{eq}$ is the equivalent shear rigidity:

$$(AG)_{eq} = \frac{bd^2 G_c}{c} \approx bdG_c \tag{3}$$

in terms of the geometric parameters defined in the preceding sub-section, and of the distance between the centroids of the faces $d = c + t_f$.

2.2. Strength

Four main modes of collapse have been identified for sandwich beams in three-point and four-point bending: (i) face yield or face microbuckling, (ii) wrinkling of the compressive face sheet, (iii) core shear, and (iv) indentation beneath the loading rollers, as shown in Fig. 2. These modes of sandwich beam collapse have been confirmed by a number of studies including those of Triantafillou and Gibson [9,10], Gibson and Ashby [4], Lingaiah and Suryanarayana [11], Zenkert [1], Theotokoglou [12], and Chen et al. [5]. Simple analytical expressions can be stated for the collapse load associated with each mode. The expressions given below for face yield/face microbuckling, for core shear and for face wrinkling are well-established; see for example Zenkert [1]. However, that for indentation

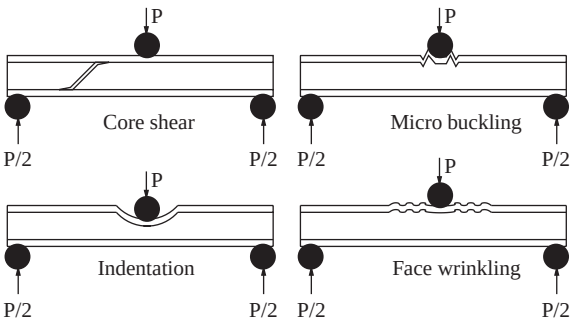

Fig. 2. Failure modes of a sandwich beam in three-point bending.

is novel and has been detailed in the companion paper [8]. For a sandwich beam in three-point bending, as in Fig. 1, the predicted collapse loads are, for face yielding or microbuckling:

$$P = \frac{4\sigma_f b t_f d}{L} \tag{4}$$

for core shear failure:

$$P = 2\tau_c b d \tag{5}$$

for face wrinkling:

$$P = \frac{2bt_f d}{L}\sqrt[3]{E_f E_c G_c} \tag{6}$$

and for indentation:

$$P = bt_f\left(\frac{\pi^2\sigma_c^2 E_f d}{3L}\right)^{1/3}. \tag{7}$$

The indentation model assumes that the compressive sandwich face behaves as an elastic beam—column, with the core as a rigid—ideally plastic foundation. A more sophisticated version of this model assumes that the core behaves in an elastic-ideally plastic manner; see Steeves and Fleck [8] for full details. In the present study we will assess the accuracy of the indentation models of Steeves and Fleck [8] by comparing the predictions with the measured indentation response and with finite element calculations for glass fibre-epoxy face sheets and PVC foam cores.

2.3. Failure mechanism maps

The above formulae for the competing collapse modes of a sandwich beam in three point bending can be used to construct a failure mechanism map. The map takes as axes the ratio of core thickness c to span L, and the ratio of face sheet thickness t_f to core thickness c; thus, the map displays all possible beam geometries for a given material combination. Regimes of dominance of collapse mechanism can be displayed, together with contours of non-dimensional collapse load, mass of sandwich beam, and so on. The experimental investigation of the present study focuses on sandwich beams with a Divinycell H100 foam and Fibredux glass fibre-epoxy faces, and the collapse mechanism map for this material combination is shown in Fig. 3. The lines A–H in Fig. 3 refer to geometries used in the experimental investigation reported below in Section 5. H100 foam is a closed cell PVC foam of density 100 kg m^{-3}, while the Hexcel Fibredux face sheets comprise an 8-harness satin weave of E-glass fibres in 914G epoxy matrix. The pertinent material properties for construction of the map have been measured and are reported in full below. In summary, the core properties are $E_c = 120$ MPa, $\tau_c = 1.6$ MPa and $\sigma_c = 1.45$ MPa, while the face-sheet properties are $E_f = 30$ GPa and $\sigma_f = 350$ MPa. The measured values for Poisson's ratio of the core and faces are 0.3 and 0.18, respectively. It is apparent from Fig. 3 that the expected collapse modes are indentation beneath the central roller and core shear. Microbuckling becomes operative for denser cores, for example Divinycell H200, as discussed by Steeves and Fleck [8].

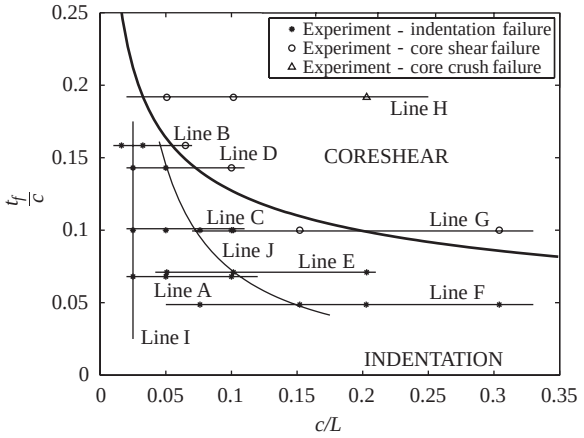

Fig. 3. Failure mode map for H100 PVC foam core and GFRP faces. The axes are the ratios of core thickness/beam length (c/L), and face thickness/core thickness (t_f/c). The solid bold line represents the boundary between the regimes of core shear and indentation failure. The lines A–J refer to sets of specimen geometry used in the experimental investigation. The data points refer to geometries tested, with the failure mode marked as '$*$' for indentation, '$\circ$' for core shear, and '$\triangle$' for core crushing.

3. Experiments

The experimental component of this study entails first a characterisation of the face and core materials, and second, three-point bending tests on sandwich beams of widely varying geometry.

3.1. Properties of sandwich beam materials

3.1.1. PVC foam core

Closed-cell Divinycell PVC foams H30, H100 and H200, with relative densities of approximately 2.6%, 6.6%, and 13.3%, were used. [1] Tension, compression, and shear tests were performed on foam samples of all three densities using a screw-driven Instron 5500R test machine. Between three and six specimens were tested for each density of foam and each loading configuration, and the typical measured responses are reported here. The scatter was found to be negligible: the peak strength in tension, compression, and shear varied by only a few per cent for nominally identical specimens.

Tension tests were conducted on dogbone specimens of gauge length 100 mm and cross-section 50 mm $\times$ 50 mm for each foam density. Loading was perpendicular to the rise direction of the foam. Tensile strains were measured using a clip gauge over a 50 mm gauge length. Nominal stress–strain curves from tests on all three foam densities are given in Fig. 4, at a nominal strain rate of 10^{-3} s^{-1}.

Compression tests were conducted on cubes of side 50 mm, with the loading direction both parallel and perpendicular to the rise direction in order to determine the degree of material anisotropy. Compressive strains were measured using a clip gauge of gauge length 12.5 mm, and the resulting nominal stress–strain curves at a strain rate of 6.7×10^{-4} s^{-1} are presented in Fig. 5. For all three

[1] We assume that the bulk density of the parent polymer is 1400 kg m^{-3}.

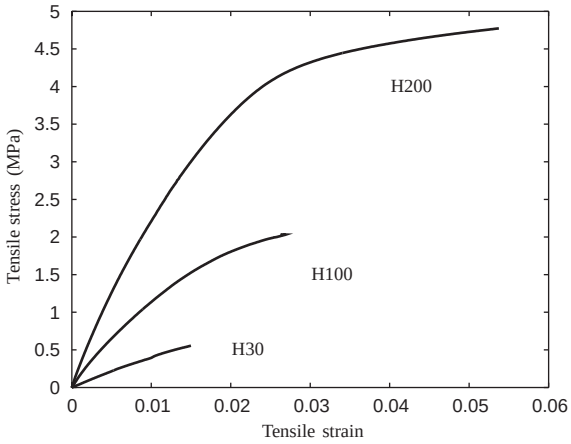

Fig. 4. Nominal stress–strain curves for typical tension tests on Divinycell PVC foams.

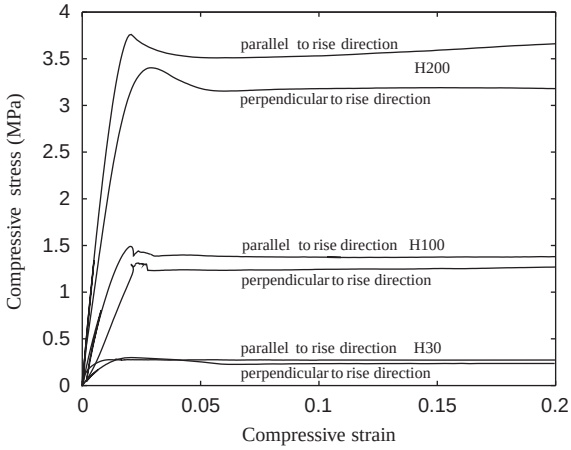

Fig. 5. Nominal stress–strain curves for typical compression tests on Divinycell PVC foams.

foam densities, the orientation parallel to the rise direction is both stiffer and stronger than that perpendicular to the rise direction.

Double lap shear tests were performed on specimens 10 mm thick, 100 mm long, and 20 mm wide for each density of foam. In specimen manufacture, the steel surfaces of the shear test rig were degreased and abraded, and the foam specimens were adhered to the grips using a two-part epoxy, Araldite, with a room-temperature cure. During the shear tests, the H200 shear specimens failed prematurely at the grips. Consequently, shear data for the H200 foam were taken from the manufacturer's data sheets [13]. The measured shear stress–strain curves for the H30 and H100 foams are shown in Fig. 6 at a shear strain rate $\dot{\gamma} = 10^{-3}\ \mathrm{s}^{-1}$. The progressive softening following peak load is due to the formation of an array of microcracks which coalesce at mid-plane to form

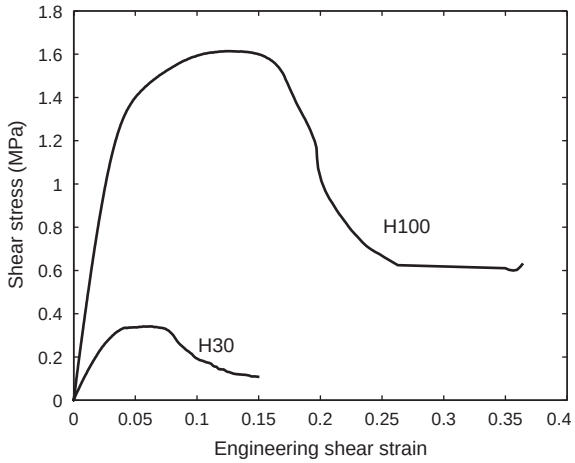

Fig. 6. Engineering shear stress–strain curves for typical shear tests on Divinycell PVC foams.

Table 1
Mechanical properties of Divinycell foams

Foam designation	H30	H100	H200
Density (kg m^{-3})	36	95	186
Compressive modulus (MPa)	26	120	280
Compressive strength (rise) (MPa)	0.25	1.45	3.5
Compressive strength (perp) (MPa)	0.24	1.3	3.2
Tensile modulus (MPa)	44	149	277
Tensile strength (MPa)	0.48	1.9	4.7
Shear modulus (MPa)	13	44	90
Shear strength (MPa)	0.33	1.6	3.3

a macroscopic mode II crack. Tensile, compressive, and shear strength and stiffness data for the foams are summarised in Table 1.

These results support the polymer foam yield surface proposed by Deshpande and Fleck [14], as follows. Fig. 7 gives plots of equivalent stress $\hat{\sigma}$ versus equivalent strain $\hat{\varepsilon}$, as defined in Appendix A, for H100 foam. According to the Deshpande–Fleck polymer foam model, the $\hat{\sigma}$ versus $\hat{\varepsilon}$ relations for tension and shear are identical, while that for compression follows the other two until a critical compressive principal stress is attained. Thereafter, the compressive response displays ideally plastic behaviour associated with elastic buckling of the cell walls (see [14]). This figure shows the expected behaviour, and supports the use of this constitutive model in the finite element modelling.

3.1.2. Woven glass-epoxy face sheets

All face sheets used in this study were manufactured from Hexcel Fibredux 7781-914G woven glass-epoxy composite prepreg. The roving in this prepreg is an E-glass 8-harness satin weave with

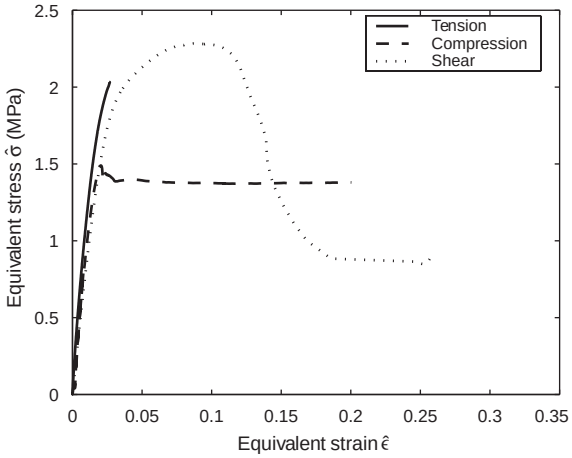

Fig. 7. Plot of equivalent stress as a function of equivalent strain for H100 polymer foam in tension, compression, and shear.

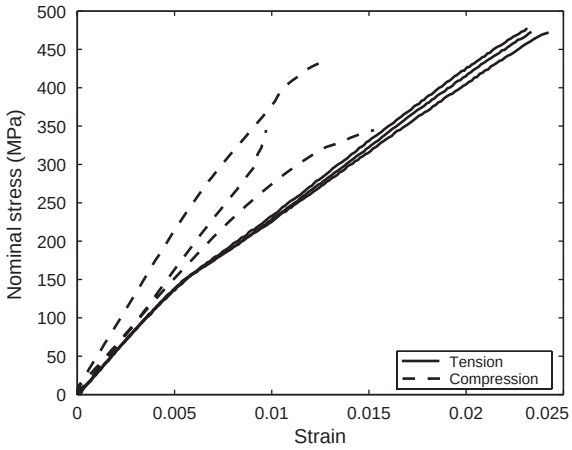

Fig. 8. Nominal stress–strain curves for tension and compression tests on Hexcel Fibredux woven glass-epoxy composite. Both tensile and compressive stresses are shown as positive.

warp and weft proportions approximately equal. Specimens for the tension tests were 1 mm thick and 10 mm wide, with a 50 mm gauge length. Aluminium tabs were bonded to the specimens using Hexcel Redux 322 epoxy. Three specimens were loaded to failure at a strain rate of 3.4×10^{-4} s^{-1} in a screw-driven Instron 5500R test frame. The nominal stress–strain curves from these tensile tests are shown in Fig. 8. Post-test visual examination of the specimens revealed that the noticeable kink in the stress–strain curve at a strain of approximately 0.005 is due to matrix cracking; this is characteristic of tensile tests on glass fibre composites. No delamination of the end tabs was detected.

Compression tests using a Celanese test rig were conducted on three specimens nominally 1 mm thick and 10 mm wide, with a gauge length of 10 mm. Strain gauges of length 2 mm were applied to both sides of the specimen, and the data for specimens with excessive bending during testing were discarded.[2] Aluminium tabs were bonded to the specimens using Hexcel Redux 322 epoxy, and the Celanese testing apparatus was used to load the specimens to failure at a cross head rate of 0.0083 mm s^{-1}. The nominal stress–strain curves for these tests are included in Fig. 8. As expected, the experimental scatter in compression tests was much greater than that in tensile tests. The average compressive strength and axial modulus of the GFRP faces were taken to be 350 MPa and 30 GPa, respectively. These values lie within the range given by the manufacturer.

3.2. Sandwich beams

3.2.1. Beam construction

Sandwich panels were assembled manually by bonding glass fibre-epoxy face sheets to H100 and H200 Divinycell PVC foam cores of thickness 6.3–30.4 mm, using a two-part room-temperature-curing polyester adhesive, designated Ciba Geigy XB 5090-1/XB 5304. The choice of face sheet thickness (in the range 0.68–3.89 mm) was dictated by the thickness of the prepreg laminae. The adhesive was applied at an areal density of approximately 0.5 kg m^{-2} and was cured at room temperature and at a 1.5 kPa dead load, with no post-cure cycle.[3] The sandwich panels were assembled with the rise direction of the foam aligned with the normal of the face sheets. Beams of width 35 mm were then cut from the sandwich panels using a diamond grit saw; the lengths of the specimens was varied from 110 to 410 mm, and included a 5 mm overhang at each end of the beam. Details of the geometries of the beams tested in this study are given in Table 2. Since a major goal of this study was the validation of the indentation model proposed by Steeves and Fleck [8], the experimental programme concentrated on sandwich geometries which favoured indentation failure.

3.2.2. Sandwich beam test method

A 120 Ω strain gauge of length 2 mm was adhered to the top face of the beam at a location 5 mm from the centre line to measure the axial strain in the compressive face. The relative sliding displacement between the faces was measured by attaching a clip gauge to the top and bottom faces of the sandwich beam mid-way between the loading roller and a support roller. This clip gauge gives an accurate estimate of shear displacement across the core since the faces remain bonded to the core and the shear strain levels within the faces are at least two orders of magnitude less than that in the core. A second clip gauge was attached directly beneath the loading roller to measure the relative approach of the faces. The full test set-up is shown in Fig. 9. The instrumented beam was loaded using a three-point bending rig with 20 mm diameter steel cylindrical rollers in a 100 kN screw-driven Instron 5500R test machine at a cross-head speed of (L/100)mm/min, where L is the span of the sandwich beam in units of mm.

[2] A longer strain gauge would have been preferable but limited access within the Celanese rig obviated this.

[3] During testing, no delamination failure of the adhesive was observed.

Table 2
Summary of sandwich beam tests

Specimen geometry	c (mm)	t_f (mm)	L (mm)	Analyt. fail. mode	Obs. fail. mode	Obs. fail. load (N)	Analyt./obs. load	FE/obs. load
A1	10	0.68	100	I	I	823	0.81	0.84
A2	10	0.68	200	I	I	564	0.94	0.93
A3	10	0.68	400	I	I	442	0.95	0.89
B1	6.5	1.03	100	C	C	873	0.97	0.99
B2	6.5	1.03	200	I	I	743	0.96	0.76
B3	6.5	1.03	400	I	I	538	1.06	0.81
C1	10	1.03	100	I	I	1049	0.95	0.94
C2	10	1.03	200	I	I	847	0.93	0.87
C3	10	1.03	400	I	I	630	0.99	0.88
D1	10	1.43	100	C	C	1408	0.91	0.78
D2	10	1.43	200	I	I/C	1118	1.02	0.88
D3	10	1.43	400	I	I	863	1.05	0.88
E1	20.3	1.44	100	I	I	1974	0.91	0.99
E2	20.3	1.44	200	I	I	1640	0.87	0.95
E3	20.3	1.44	400	I	I	1161	0.97	0.99
F1	30.4	1.48	100	I	I	2297	0.91	1.03
F2	30.4	1.48	150	I	I	1869	0.98	1.05
F3	30.4	1.48	200	I	I	1685	0.99	1.08
F4	30.4	1.48	400	I	I	1377	0.96	1.02
G1	30.4	3.04	100	C	C	3900	0.96	1.03
G2	30.4	3.04	200	I	C	2860	1.21	1.12
G3	30.4	3.04	300	I	I	3041	1.00	0.89
G4	30.4	3.04	400	I	I	2563	1.07	1.00
H1	20.3	3.89	100	CC	CC	5900	0.46	0.85
H2	20.3	3.89	200	C	C	3077	0.88	1.05
H3	20.3	3.89	400	C	C	2463	1.10	1.06
K1	6.3	0.68	100	I	I	1049	1.06	1.00
K2	6.3	0.68	200	I	I	815	1.08	0.91
K3	6.3	0.68	400	M	M	536	1.08	0.94

All cores are made from H100 foam except for specimens K1–K3, which are made from H200 foam. I = indentation mode; C = core shear mode; M = microbuckling mode; CC = core crush mode. Analyt. = analytical; Obs. = observed.

The outer steel support rollers of diameter 20 mm were fixed in position, with a small (5 mm) overhang of the ends of the specimen as mentioned above. As the beams rotated and slid past the outer rollers, the reaction force at the rollers remained normal to the beam. A small amount of indentation of the sandwich beam was evident at the outer supports.

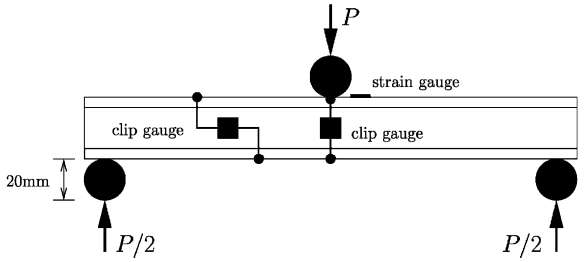

Fig. 9. Sandwich beam instrumentation.

4. Finite element predictions of beam behaviour

In addition to analytical predictions of sandwich beam stiffness and strength, finite element analysis has been used to model the behaviour of selected sandwich beams in three-point bending. The polymer foam constitutive model of Deshpande and Fleck [14] has been employed; it utilises a principal stress yield surface in compression and a quadratic yield surface elsewhere in stress space. The constitutive model has been calibrated against measured foam properties, as described in Appendix A, and the finite element implementation followed that of Chen and Fleck [15]. The polymer foam constitutive model does not account for fracture of the foam. Consequently, the finite element model is unable to predict the post-peak load response of the sandwich beam after the core has fractured in shear. Instead, the shear strain distribution in the core is extracted from the finite element model and the load at which the maximum shear strain first exceeds the fracture shear strain in the core is taken as the failure load. For the case of H100 foam, this critical shear strain is 15%, based upon the shear tests described above.

The finite element analysis package ABAQUS was used to analyse the sandwich beam response. Due to symmetry, only half of the beam was modelled. Typically, the mesh contained approximately 2000 six-noded, three-sided plane strain elements, with the core eight elements deep and the faces four elements deep. The justification for the choice of plane strain elements is as follows. The foam core is constrained by the face sheets and behaves in an approximately plane strain manner. The faces are much wider than their thickness, and anti-clastic curvature is constrained by the cylindrical rollers. Thus, the simple plane strain assumption seems appropriate, although a full 3-D study is needed to resolve fully the accuracy of this assumption; such a study is beyond the scope of the present investigation. Appropriate mesh refinements near the contacts between the beam and loading rollers were included. A typical mesh is shown in Fig. 10. Both geometric and material non-linearity were modelled, and the calculation was performed by prescribing an increasing displacement of the mid-point loading roller. Contact between the sandwich beams and the three rigid circular rollers was handled by a contact algorithm within ABAQUS. In order to achieve numerical convergence, a small value of Coulomb friction coefficient of $\mu = 0.01$ was assumed. Numerical experimentation confirmed that the precise value of μ had a negligible effect upon the response.

The face sheets were treated as isotropic, elastic—ideally plastic with Poisson's ratio 0.18, and tensile and compressive yield strengths equal to the microbuckling strength. The finite element calculations confirmed that the assumed yield strength of the face sheets was attained only for the collapse mode of face microbuckling; in that case, the failure load was taken at the point when

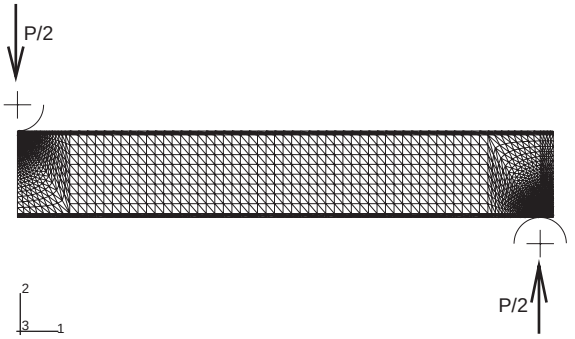

Fig. 10. Typical finite element mesh for sandwich beam.

yielding had spread through the thickness of the face sheet immediately beneath the loading roller. It is argued that the assumption of isotropy is acceptable because the transverse stress generated in the face sheets is negligible compared with the axial stress.

5. Experimental results and comparison with analytical and finite element predictions

We begin by giving detailed experimental results and predictions for three representative sandwich beams—one failing by core shear, one by face sheet microbuckling and one by indentation. Second, the effect of a systematic variation in sandwich beam geometry upon the peak strength is determined experimentally, and compared with both finite element predictions and analytical estimates from Eqs. (4), (5) and (7). The chosen sandwich geometries for the Divinycell H100 PVC foam core are displayed in Fig. 3. A few additional tests were performed using a higher density foam H200 in order to attain fibre microbuckling as a failure mode. The full list of geometries tested is summarised in Table 2. Third, the experimental results for each failure mode are assembled and compared with the finite element and analytical predictions.

5.1. Typical collapse responses

It is instructive to compare the experimental results for three sandwich beams, designated H2, K3 and F4 in Table 2, which collapse by core shear, fibre microbuckling of the compressive face sheet, and indentation, respectively. The measured load P on the mid-roller versus the mid-roller displacement u is plotted in Figs. 11–13 for each geometry in turn. Additionally, the predictions of the finite element simulations and the analytical formulae for stiffness and strength (for the observed collapse mode) are included in the figures. We consider each specimen in turn.

5.1.1. Core shear

Consider first the measured response and predictions for specimen H2, which failed by core shear. In broad terms, the analytical and finite element predictions both give adequate estimates for the initial stiffness, and for the peak strength. The analytical model for collapse by core shear slightly underpredicts the peak strength since it neglects the contribution of the face sheets to the bending

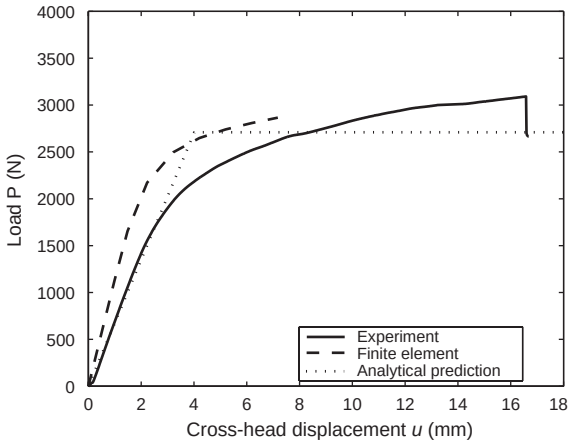

Fig. 11. Measured and predicted load P versus cross-head displacement u, for sandwich beam H2 failing by core shear.

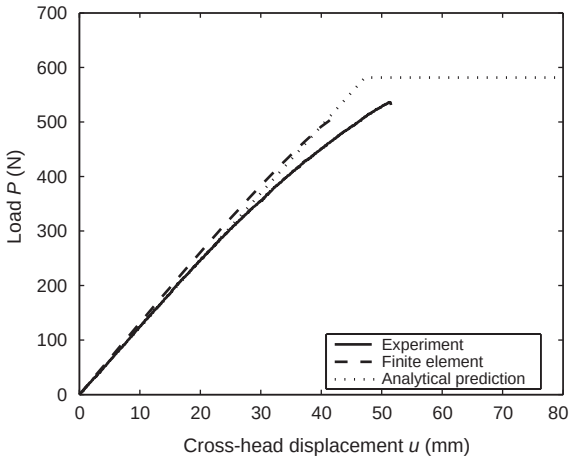

Fig. 12. Measured and predicted load P versus cross-head displacement u, for sandwich beam K3 failing by microbuckling of the compressive face.

strength. The finite element simulations confirm that the shear strain distribution within the core is almost constant between the mid-roller and the outer supports. However, the finite element analysis does not take into account the progressive development of macroscopic shear cracks within the core, and so failure is predicted at a cross-head displacement of about half the observed value. (In the finite element calculations, core shear failure is defined as the point when the maximum shear strain in the core attains the critical value of 15%.) Fig. 14 compares the evolution of measured shear strain in the core (via the shear clip gauge as shown in Fig. 9) with the average shear strain predicted by the finite element simulation: good agreement is obtained.

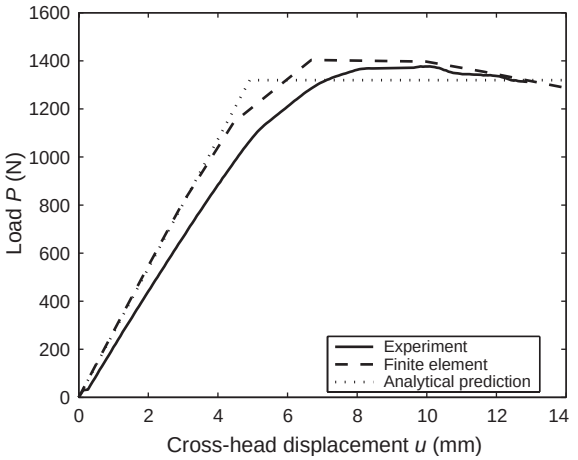

Fig. 13. Measured and predicted load P versus cross-head displacement u, for sandwich beam F4 failing by indentation.

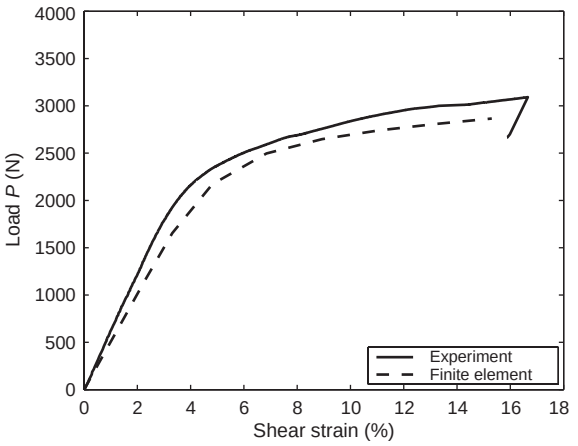

Fig. 14. Measured and predicted load P versus average shear strain across the core section, for sandwich beam H2 failing by core shear.

5.1.2. Face sheet microbuckling

In order to achieve face sheet microbuckling it was found necessary to manufacture and test a sandwich beam containing a high density H200 Divinycell core (designated K3 in Table 2). Face sheet microbuckling is a catastrophic event within the face sheets and gives rise to a sudden drop in load carrying capacity, as is evidenced by the measured load versus displacement response at the mid-roller shown in Fig. 12. Prior to microbuckling the observed and predicted responses are almost linear; it is clear from Fig. 12 that both the analytical and finite element calculations give accurate predictions of the stiffness and strength of the sandwich beam. The compressive strain in the top face sheet has been measured by an axial strain gauge located adjacent to the mid-roller. As an additional check, the strain history detected by this gauge is compared in Fig. 15 with the finite element prediction for the same location. Again, excellent agreement is evident.

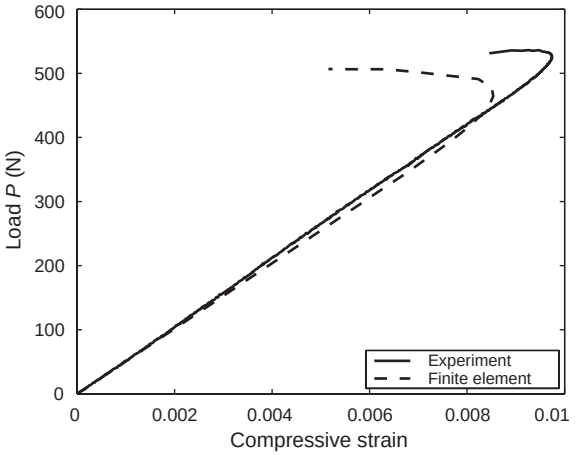

Fig. 15. Measured and predicted top face compressive strain versus load P, for sandwich beam K3 failing by microbuckling of the compressive face.

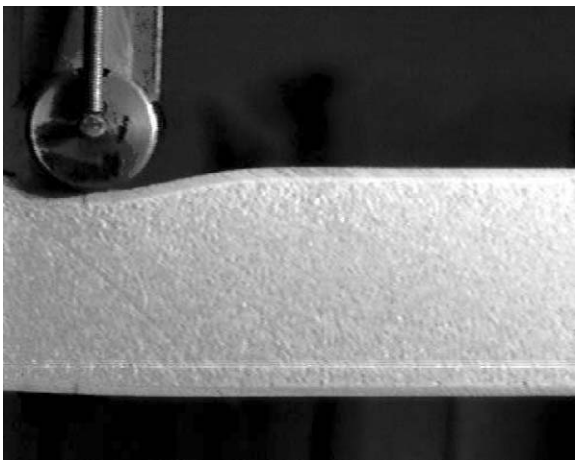

Fig. 16. Video capture of sandwich beam F4, failing by indentation.

5.1.3. Indentation

The finite element and analytical models each give acceptable agreement with the measured indentation collapse response of specimen F4, see Fig. 13. A load maximum is observed with mild softening thereafter; both the finite element calculations and the analytic model developed by Steeves and Fleck [8] predict this form of collapse response. Also, the finite element simulations confirm that the axial stress in the upper face sheet remains below the microbuckling strength. Video recordings of the deflected shape of the upper face sheet confirms that the sandwich beam F4 failed by local indentation; a typical image from the video recording is shown in Fig. 16. Additional confirmation of the indentation mechanism is provided by plotting in Fig. 17 the load P on the mid-roller against the relative approach of the two face sheets between the roller, as measured by a clip gauge straddling

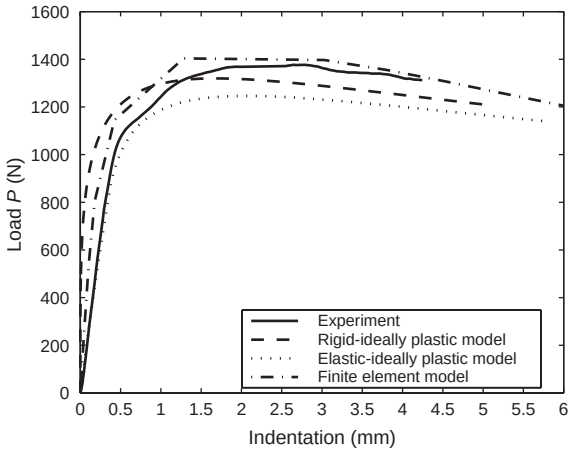

Fig. 17. Measured and predicted load P against indentation depth, for sandwich beam F4 failing by indentation.

the faces. The plot also contains the finite element prediction of load versus relative displacement of faces, and analytic estimates of the load versus indentation depth for an elastic column upon a rigid-ideally plastic foundation and upon an elastic-ideally plastic foundation, taken from Steeves and Fleck [8]. All three predictions give accurate estimates of the peak load at an indentation depth of approximately 2 mm; the finite element model appears to be the most accurate in reproducing the load versus indentation depth response. As expected, the column-buckling model with a rigid—ideally plastic foundation predicts too stiff an initial response, but is satisfactory in other respects.

Measured and predicted peak loads, and the associated collapse modes, are summarised in Table 2 for all sandwich beams tested. All beams except for specimen G2 failed by the predicted mode. Specimen G2 lies close to the core shear-indentation boundary (see Fig. 3) and collapsed predominantly by core shear instead of the predicted mode of indentation. The operative collapse mode is sometimes difficult to detect: core shear and indentation can occur simultaneously when the sandwich geometry lies close to the boundary of the two modes.

5.2. Effect of sandwich beam geometry upon collapse mode and strength

In order to validate the analytical models and finite element analysis for the prediction of sandwich beam strength, a systematic set of experiments have been performed by varying the beam span L, core thickness c and face sheet thickness t_f. The failure mode map shown in Fig. 3 contains points representing the geometries tested with a H100 foam core. There are 10 lines, labelled A–J, representing trajectories over which the functional relationship between failure load and geometric parameters have been explored. Lines A–H are paths of varying beam length, line I is a path of varying face thickness, and line J is a path of varying core thickness. The failure loads predicted by the analytical models and the finite element analysis are compared with the measured failure loads for the selected trajectories F, G, and H, and also for trajectories I and J.

Fig. 18 shows predicted and observed failure loads for trajectory F of Fig. 3. This trajectory is for a varying beam length with constant face thickness $t_f = 1.48$ mm and constant core thickness

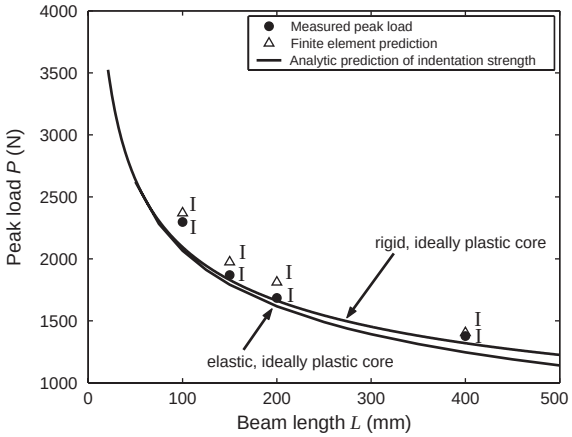

Fig. 18. Predicted and observed failure loads for trajectory F: H100 core, $c = 30.4$ mm, $t_f = 1.48$ mm and I = indentation.

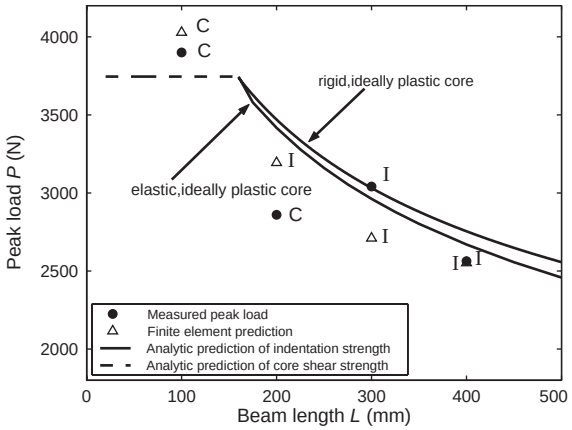

Fig. 19. Predicted and observed failure loads for trajectory G: H100 core, $c = 30.4$ mm, $t_f = 3.04$ mm; I = indentation and C = core shear.

$c = 30.4$ mm. The specific beam geometries are given by specimens F1, F2, F3, and F4 in Table 2. As can be seen from the failure mode map, Fig. 3, these geometries fall well within the indentation region, and all these beams failed by indentation. Quantitative agreement is evident between the finite element models, the analytical predictions, and the measured strengths.

Next, the predicted and observed failure loads for trajectory G of Fig. 3 are compared in Fig. 19. This trajectory is again for a varying beam length with constant face thickness $t_f = 3.04$ mm and constant core thickness $c = 30.4$ mm, representing geometries G1, G2, G3, and G4 in Table 2. The longer beams G3 and G4 failed by indentation, and both the finite element and analytical predictions are reasonably accurate (within 15%). The shortest beam G1 underwent core shear, with the analytical prediction slightly below the measured strength. This beam has relatively thick faces, and so it is anticipated that face bending is important: it is expected that the use of Timoshenko

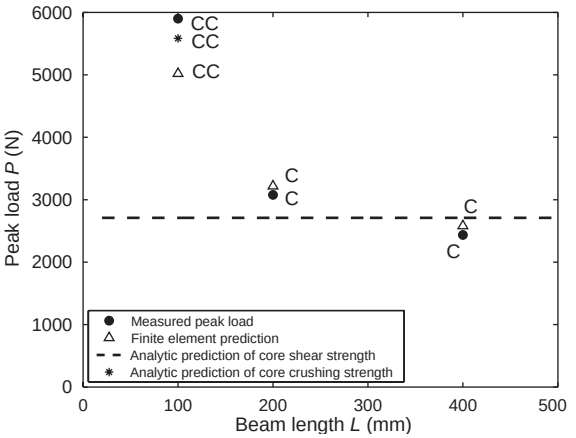

Fig. 20. Predicted and observed failure loads for trajectory H: H100 core, $c = 20.3$ mm, $t_f = 3.89$ mm; C = core shear and CC = core crushing.

beam theory for the sandwich beam would give more accurate predictions, as has been discussed by Chiras et al. [7] and Steeves and Fleck [8]. The analytical predictions suggest that the beam G2 of length $L = 200$ mm should fail by indentation; in reality it failed by core shear at an abnormally low load. This low strength is associated with the statistical scatter in core strength.

The strengths of the beam geometries H1–H3 are plotted in Fig. 20: these geometries have a constant face thickness $t_f = 3.89$ mm and a constant core thickness $c = 20.3$ mm. Geometries H2 and H3 underwent core shear, and the collapse loads predicted by the finite element simulations and by the core shear model are in good agreement with the observed strengths. The shortest beam, H1 of length $L = 100$ mm, failed by core crushing.

The core crush mode intervenes for sandwich beams with short spans and thick face sheets; then, the beam approximation fails. The core crush mode entails the upper and lower face sheets behaving as rigid platens with the core crushing between them. An estimate for the core crush load is

$$P = \sigma_c b(L + 2H). \tag{8}$$

For the case of beam geometry G1 with $\sigma_c = 1.45$ MPa, $b = 35$ mm, $L = 100$ mm, and $H = 5$ mm, the computed core crush load is 5583 N, in acceptable agreement with the measured value of 5900 N. The experimental data presented in Figs. 18–20 suggests that the core crush mode intervenes for $t_f/L > 0.04$, for the material combination employed here.

The analytical and finite element predictions are compared in Fig. 21 with the measured peak loads for geometries along trajectory I of Fig. 3. This path denotes a varying face thickness with constant beam length $L = 400$ mm and constant core thickness $c = 10$ mm and comprises geometries A3, C3 and D3 of Table 2. Collapse is by face sheet indentation, and the analytical and finite element predictions are in good agreement with the measured failure loads for these geometries.

Fig. 22 shows the predicted and observed failure loads for trajectory J of Fig. 3. Along this path the core thickness varies, with constant beam length $L = 200$ mm and face thickness $t_f \approx 1.5$ mm. These geometries are denoted by D2, E2 and F3 in Table 2. The analytical and finite element predictions all lie very close to the measured responses. The beam D2 with a 10 mm thick core

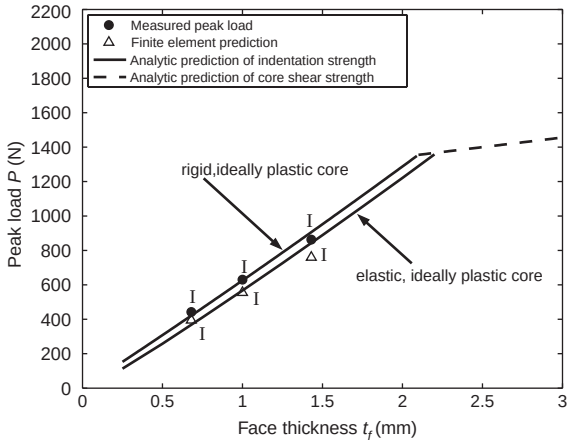

Fig. 21. Predicted and observed failure loads for trajectory I: H100 core, $c = 10$ mm, $L = 400$ mm and I = indentation.

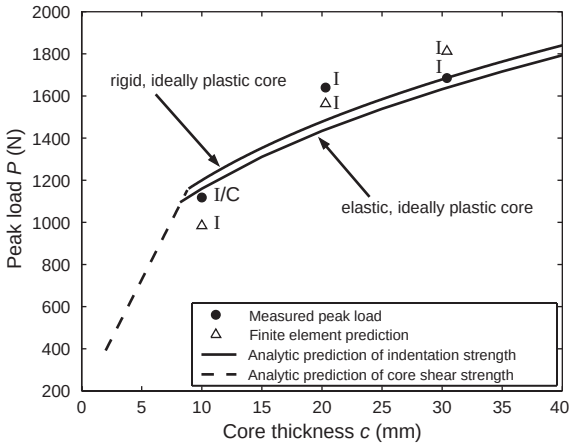

Fig. 22. Predicted and observed failure loads for trajectory J: H100 core, $t_f = 1.5$ mm, $L = 200$ mm; I = indentation and I/C = combined indentation and core shear.

failed by a combination of indentation and core shear; this is to be expected as this beam lies close to the boundary between indentation and core shear; see Fig. 3.

5.3. Accuracy of models for each failure mode

It is instructive to collect together the experimental results for each collapse mode and to compare the analytic predictions with the measured peak strengths.

5.3.1. Core shear

Core shear failure is observed in sandwich beams with relatively thick faces and small spans. The prediction given by Eq. (5) suggests that the peak load scales linearly with $d \equiv t_f + c$ for a given

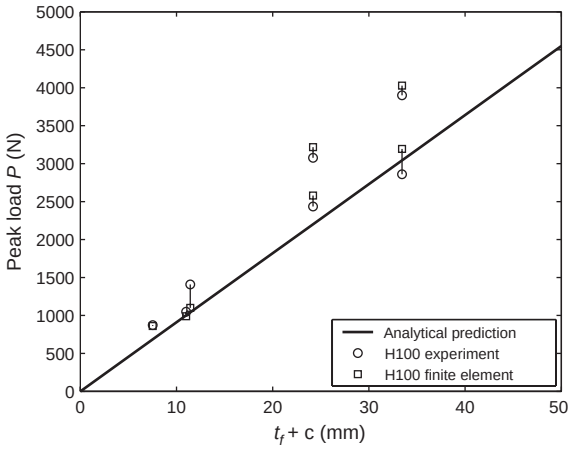

Fig. 23. Measured and predicted peak load by Eq. (5) for failure of sandwich beam by core shear. The vertical tie lines connect the finite element predictions to the corresponding experimental measurement.

combination of materials. Fig. 23 explores the accuracy of the failure load as predicted by Eq. (5) and by finite element analysis for the H100 core and GFRP faces. In two cases the measured failure load much exceeds the analytic prediction; these are short beams where failure was dominated by core crushing. In general, the analytical prediction is lower than the measured strength; this suggests that the core shear model can be improved by using Timoshenko theory to analyse the sandwich beams, as described by Chiras et al. [7]. The load versus displacement plots given in Fig. 11 support this: the numerical prediction of peak load, which includes a contribution from the bending stiffness of the faces, is more accurate than the analytic prediction.

5.3.2. *Microbuckling*

Fibre microbuckling of the compressive face occurs for very long beams with dense cores and thin faces. In this study, microbuckling was observed for a single beam, designated K3 in Table 2, with a 6.3 mm thick H200 core, 0.68 mm thick faces, and a length of 400 mm. The predicted strengths by Eq. (4) and by the finite element analysis are within 10% of the measured strength which, given the variability of the strength of composites in compression, is acceptable.

5.3.3. *Indentation*

Indentation is the active failure mode for long beams with thin faces and weak cores. The indentation model, Eq. (7), predicts that the peak load P scales linearly with $t_f((t_f + c)/L)^{1/3}$. Fig. 24 compares analytic and finite element predictions of peak loads with measured values for the H100 and H200 foams, and adopts the metric $t_f((t_f + c)/L)^{1/3}$ as the abscissa. For the beams tested, the analytical and numerical prediction are both in good agreement with the measured peak loads, and the relationship between the measured peak load and $t_f((t_f + c)/L)^{1/3}$ is indeed linear. We conclude that the Steeves–Fleck model for sandwich indentation is both physically sound and accurate for sandwich beams with polymer foam cores and composite faces.

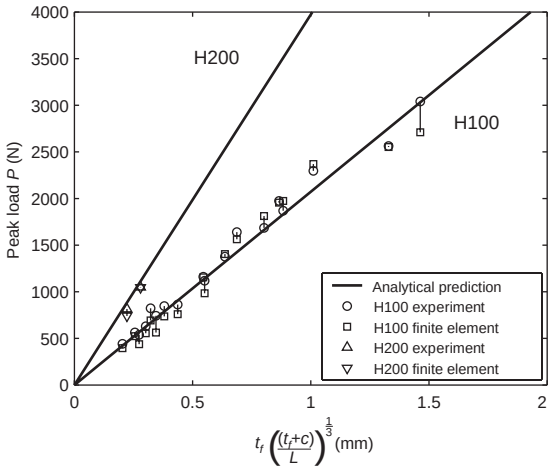

Fig. 24. Measured and predicted peak load by Eq. (7) for failure of sandwich beam by indentation. The vertical tie lines connect the finite element predictions to the corresponding experimental measurement.

6. Concluding remarks

A systematic series of experiments has been conducted on sandwich beams in three point bending, with woven glass fibre composite faces and PVC foam cores. Collapse is by core shear, face microbuckling, face sheet indentation or by core crushing, depending upon the sandwich beam geometry and the choice of density of the foam core. A failure mechanism map, with axes given by the slenderness ratio of the beam and the relative thickness of face sheet to core, is useful for showing the dominant regimes of each collapse mode, and for planning sets of experiments on the effect of beam geometry upon collapse strength. The experiments conducted herein provide support for the analytic models of collapse, and highlight the importance of indentation as a potential collapse mode. Previous investigations on sandwich beams (for example [9,16,17]) have focused on core shear; wide loading plates rather than rollers were used to prevent indentation. Although the analytical models of collapse are useful for the construction of collapse mechanism maps, closer agreement with the measured responses is obtained by detailed finite element calculations. For this purpose, the Deshpande and Fleck [14] constitutive description for a polymer foam has been implemented within the ABAQUS standard finite element program and has been calibrated with the stress–strain curves for PVC foams in tension, compression and shear. The finite element simulations are able to capture the structural response of the sandwich beams up to the point of fracture of the core (core shear mode) or of the faces (microbuckling).

Acknowledgements

The authors are grateful for financial support from the US Office of Naval Research, contract 0014-91-J-1916. The authors also thank Mr. John Ellis of Hexcel Composite Materials, Duxford, UK for providing the glass fibre prepregs and manufacturing facilities.

Appendix A. Constitutive model of polymer foams

In the finite element analysis of the present study, Divinycell PVC foam is modelled as an isotropic porous solid, with the constitutive description of Deshpande and Fleck [14]. Tensile yield of the foam is governed by an elliptical yield surface in von Mises stress σ_e versus mean stress σ_m space, while in compression the cell walls buckle elastically, and a maximum principal stress criterion applies. A visco-plastic version of the model has been implemented within the finite element code ABAQUS, using the user subroutine interface UMAT [15].

In the visco-plastic formulation of the Deshpande–Fleck constitutive model, the overall creep potential Φ is taken as

$$\Phi = \Phi_1 + \Phi_2 + \Phi_3 + \Phi_H, \tag{A.1}$$

where Φ_i $(i = 1, 3)$ are individual creep potentials associated with the three principal stresses σ_i and the potential Φ_H is elliptical in stress space, such that:

$$\Phi_i = \frac{\dot{\varepsilon}_{i0}\sigma_{i0}}{n_i + 1}\left|\frac{\sigma_i}{\sigma_{i0}}\right|^{n_i+1} H(-\sigma_i) \quad \text{(no summation on } i\text{)} \tag{A.2}$$

and

$$\Phi_H = \frac{\dot{\hat{\varepsilon}}_0\hat{\sigma}_0}{n_H + 1}\left(\frac{\hat{\sigma}}{\hat{\sigma}_0}\right)^{n_H+1}. \tag{A.3}$$

$H(\cdot)$ is the Heaviside step function, and the material parameters $(\sigma_{i0}, \dot{\varepsilon}_{i0}, n_i)$ and $(\hat{\sigma}_0, \dot{\hat{\varepsilon}}_{i0}, n_H)$ are determined as follows.

First, the exponents n_i and n_H are set to the large value of 10 in order to give a compromise between numerically stable solutions and minimal rate sensitivity. Second, the material parameters σ_{i0} and $\dot{\varepsilon}_{i0}$ are measured in a uniaxial compression test, such that $\dot{\varepsilon}_{i0}$ is the applied uniaxial strain rate and σ_{i0} is the measured plateau stress. It is assumed that the foams behave isotropically, such that $\sigma_{10} = \sigma_{20} = \sigma_{30}$. Third, the material parameters $\hat{\sigma}_0$ and $\dot{\hat{\varepsilon}}_0$ are obtained from a shear test, as shown in Fig. 6. The parameter $\hat{\sigma}_0$ has the interpretation of a uniaxial tensile yield strength at the uniaxial strain rate $\dot{\hat{\varepsilon}}_0$. Since the Divinycell foams had a low ductility in tension and a much higher ductility in shear, the value of $\hat{\sigma}_0$ was derived from the peak shear strength τ_{max}. Recall that the Deshpande and Fleck [14] model relates any stress state, as characterised by the von Mises stress σ_e and the mean stress σ_m, to an equivalent stress $\hat{\sigma}$ according to

$$\hat{\sigma}^2 = \frac{\sigma_e^2 + \alpha^2\sigma_m^2}{1 + \alpha^2/9}, \tag{A.4}$$

where α is a material constant. The parameter α dictates the shape of the quadratic yield surface, and can be related directly to the plastic Poisson's ratio v^p (the negative ratio of the radial plastic strain rate to the axial plastic strain rate in a uniaxial tension test) by

$$\alpha^2 = \frac{9(1 - 2v^p)}{2(1 + v^p)}. \tag{A.5}$$

Table 3
Values of ABAQUS UMAT code input parameters for polymer foam constitutive model

	E (MPa)	v	n	$\hat{\sigma}_0$ (MPa)	σ_{i0} (MPa)	$\dot{\hat{\varepsilon}}_0$ (s^{-1})	$\dot{\hat{\varepsilon}}_{i0}$ (s^{-1})
H100	150	0.3	10	2.28	1.45	0.00066	0.00066
H200	280	0.3	10	4.67	3.5	0.00066	0.00066

For polymeric foams, the plastic Poisson's ratio v^p is approximately zero; see for example Deshpande and Fleck [14] or Gibson and Ashby [4]. This implies that $\alpha = 2.12$. The equivalent strain rate $\dot{\hat{\varepsilon}}$ is related to the von Mises effective strain rate $\dot{\varepsilon}_e$ and to the hydrostatic strain rate $\dot{\varepsilon}_H = \dot{\varepsilon}_{kk}$ by

$$\dot{\hat{\varepsilon}}_e^2 = \left(1 + \frac{\alpha^2}{9}\right)\left(\dot{\varepsilon}_e^2 + \frac{1}{\alpha^2}\dot{\varepsilon}_H^2\right). \tag{A.6}$$

For the case of simple shear, the shear stress on the foam is a measured function of the plastic shear strain γ^p, and we have $\sigma_e = \tau\sqrt{3}$ and $\dot{\varepsilon}_e = \dot{\gamma}^p/\sqrt{3}$. This leads to the identity $\hat{\sigma}_0 = \tau_{max}\sqrt{2}$ at the applied strain rate $\dot{\hat{\varepsilon}}_0 = \dot{\gamma}^p/\sqrt{2}$. The material parameters $\hat{\sigma}_0$ and $\dot{\hat{\varepsilon}}_0$ are thereby derived. The experimental results reported above in Section 3 give rise to the material parameters listed in Table 3.

References

[1] Zenkert D. An introduction to sandwich construction. Sheffield, UK: Engineering Materials Advisory Service; 1995.
[2] Allen H. Analysis and design of structural sandwich panels. Oxford: Pergamon Press; 1969.
[3] Plantema F. Sandwich construction. New York: Wiley; 1966.
[4] Gibson L, Ashby M. Cellular solids. Cambridge: Cambridge University Press; 1988.
[5] Chen C, Harte A-M, Fleck N. The plastic collapse of sandwich beams with a metallic foam core. International Journal of Mechanical Sciences 2001;43(6):1483–506.
[6] McCormack T, Miller R, Kesler O, Gibson L. Failure of sandwich beams with metallic foam cores. International Journal of Solids and Structures 2001;38(28–29):4901–20.
[7] Chiras S, Mumm D, Evans A, Wicks N, Hutchinson J, Dharmasena H, Wadley H, Fichter S. The structural performance of near-optimized truss core panels. International Journal of Solids and Structures 2002;39(15): 4093–115.
[8] Steeves C, Fleck N. Collapse mechanisms of sandwich beams with composite faces and a foam core, loaded in three-point bending. Part I: Analytical models and minimum weight design. International Journal of Solids and Structures, 2004, in press, doi:10.1016/j.ijmecsci.2004.04.003
[9] Triantafillou T, Gibson L. Failure mode maps for foam core sandwich beams. Materials Science and Engineering 1987a;95:37–53.
[10] Triantafillou T, Gibson L. Minimum weight design of foam core sandwich panels for a given strength. Materials Science and Engineering 1987b;95:55–62.
[11] Lingaiah K, Suryanarayana B. Strength and stiffness of sandwich beams in bending. Experimental Mechanics 1991;31(1):1–7.
[12] Theotokoglou E. Analytical determination of the ultimate strength of sandwich beams. Applied Composite Materials 1996;3:345–53.
[13] Divinycell. Divinycell Technical Specification H Grade. Technical report, DIAB, 1997.
[14] Deshpande V, Fleck N. Multiaxial yield behaviour in polymer foams. Acta Materialia 2001;49(10):1859–66.

[15] Chen C, Fleck N. A creep model for polymeric foams. Technical Report CUED/C-MICROMECH/TR.32, Cambridge Centre for Micromechanics, University of Cambridge, 2000.
[16] Burman M, Zenkert D. Fatigue of foam core sandwich beams—1: undamaged specimens. International Journal of Fatigue 1997a;19(7):551–61.
[17] Burman M, Zenkert D. Fatigue of foam core sandwich beams—2: effect of initial damage. International Journal of Fatigue 1997b;19(7):563–78.